

# 光学学报

## 煤炭行业甲烷排放卫星遥感研究进展与展望

秦凯\*, 何秦, 康涵书, 胡玮, 鹿凡, 科恩·杰森

中国矿业大学环境与测绘学院江苏省煤基温室气体减排与资源化利用重点实验室, 江苏 徐州 221116

**摘要** 煤炭开采是我国最主要的甲烷排放源之一,建立高时空分辨率的甲烷排放清单是推动煤炭行业甲烷减排的重要抓手。以 Sentinel-5P/TROPOMI、GHGSat-D/WAF-P、GF-5/AHSI 为代表的遥感卫星已成功用于区域和点源尺度的煤炭行业甲烷排放检测与量化研究。介绍当前可用于煤炭行业甲烷排放研究的遥感卫星及数据,分析相应的甲烷柱浓度及排放速率遥感反演技术进展,并讨论其适用性与优缺点。建议以煤矿聚集区和单一煤矿为两个关键尺度,加快建设中国煤炭行业的“自上而下”甲烷排放清单,指出未来需要重点研究的 3 点内容:采用 TROPOMI 数据和简化质量平衡法,反演全国 14 个大型煤炭基地的甲烷排放;基于 10 nm 分辨率的高光谱遥感卫星,检测与量化全国数千家煤矿的甲烷排放量;挖掘不同尺度遥感卫星观测之间的内在联系,开展协同分析。

**关键词** 甲烷; 煤矿; 排放; TROPOMI 卫星; 高分五号卫星

**中图分类号** X831 **文献标志码** A

**DOI:** 10.3788/AOS231293

### 1 引言

自工业革命以来,约 30% 的全球气温上升是甲烷造成的<sup>[1]</sup>。尽管甲烷在大气的占比很小,但作为一种强效温室气体,其全球增温潜势(GWP,即在地球大气中捕获热量的能力)在 20 年内大约是二氧化碳的 80 多倍<sup>[2]</sup>。同时甲烷分解速度比二氧化碳快得多,平均寿命(即在大气中的存续时间)约为 12 年<sup>[3]</sup>,而二氧化碳的平均寿命为上百年<sup>[4-5]</sup>。这意味着相较二氧化碳减排,甲烷的减排能在短期内起到较好控制温升的效果,产生显著的气候效益,是减缓温室效应的有力杠杆<sup>[6]</sup>。此外,甲烷还是对流层臭氧(O<sub>3</sub>)的前体物<sup>[7-8]</sup>,其减排举措的实施也有利于减少空气污染,改善空气质量。2021 年 11 月举行的第二十六届联合国气候变化框架公约缔约方会议(COP26)中,中美两国发布了《中美关于在 21 世纪 20 年代强化气候行动的格拉斯哥联合宣言》,着重强调了甲烷排放对升温的显著影响,认为加大行动控制和减少甲烷排放是 21 世纪 20 年代的必要事项<sup>[9]</sup>。

煤炭开采活动中,赋存于煤层中的甲烷以多种方式释放,包括:从露天矿的煤层中逸散;井工煤矿通过通风和抽采将甲烷排出;滞留在煤基质中的甲烷在采矿作业后期活动中(如加工、储存和运输)继续逸散;废弃矿井内的甲烷继续从作业结束后残留的煤中逸

出<sup>[10]</sup>。国际能源署数据显示,2022 年,全球煤矿甲烷的排放量约为 4050 万吨,占人为甲烷排放总量的 10% 以上<sup>[1]</sup>。我国是世界上最大的煤炭生产国,根据《中华人民共和国气候变化第二次两年更新报告》<sup>[11]</sup>的 2014 年国家温室气体清单,我国能源行业的甲烷排放占总排放的比例约为 46%,其中主要是煤炭开采产生的排放。研究表明,全球人为甲烷排在 2000 年到 2012 年的增加<sup>[12]</sup>,中国甲烷排放量从 2010 年到 2015 年的增加<sup>[13]</sup>,很大程度上是中国煤矿开采行业的贡献。加快建设煤炭行业可动态更新的高时空分辨率甲烷排放清单,是推动煤炭行业甲烷减排的重要抓手。煤矿甲烷排放会因矿井含气量、生产率、煤层渗透性及其他因素而有很大差异,每个煤矿单位煤炭产量的甲烷排放量即排放因子差异很大,传统的自下而上清单方法误差较大<sup>[14]</sup>。

利用甲烷在 1.65 μm 和 2.3 μm 的短波红外吸收光谱<sup>[15-16]</sup>,卫星遥感技术已被成功用于煤炭行业甲烷排放检测与量化。文献<sup>[17]</sup>从 GOSAT/TANSO-FTS 数据发现 2010—2017 年中国各地区的煤炭行业甲烷排放呈现不同趋势:西南地区下降;华北地区总体上升,但山西南部的沁水盆地出现下降。文献<sup>[18]</sup>使用 GHGSat-D/WAF-P 检测和量化了美国、澳大利亚和中国 3 个国家的煤矿甲烷排放羽流。2022 年 11 月的 COP27 会议上,联合国环境规划署(UNEP)的国际

收稿日期: 2023-07-20; 修回日期: 2023-08-18; 录用日期: 2023-08-22; 网络首发日期: 2023-08-30

基金项目: 国际碳卫星观测数据分析合作计划(131211KYSB20180002)、山西省科技重大专项计划揭榜挂帅项目(202101090301013)

通信作者: \*wjjs0011@cumt.edu.cn

甲烷排放观测组织 (IMEO) 启动了“甲烷预警和响应系统”。该系统先采用 TROPOMI 卫星在全球范围内查明大的甲烷排放羽流和热点, 然后利用 PRecursores IperSpettrale della Missione Applicativa (PRISMA)、Environmental Mapping and Analysis Program (EnMAP) 等具有更高分辨率的遥感卫星数据进行排放归因, 煤炭行业的甲烷排放检测是其主要目标之一。

煤炭行业甲烷排放的卫星遥感检测需要传感器、算法与探测目标之间的密切配合。本文分析可用于煤炭行业甲烷排放研究的遥感卫星情况、相应的甲烷柱浓度及排放速率遥感反演技术等方面的研究进展, 并提出面向构建高时空分辨率中国煤炭行业甲烷排放清单的卫星遥感研究重点。

## 2 可用于煤炭行业甲烷排放研究的遥感卫星

遥感卫星可以利用短波红外波段的太阳后向散射信号, 根据甲烷在  $1.65 \mu\text{m}$  波段 ( $1.63\sim 1.70 \mu\text{m}$ ) 或  $2.3 \mu\text{m}$  波段 ( $2.2\sim 2.4 \mu\text{m}$ ) 的吸收特征, 对大气中的甲烷柱浓度进行反演<sup>[19]</sup>。根据遥感卫星检测煤炭行业甲烷排放能力的空间尺度大小, 可将遥感卫星分为区域型和点源型。区域型遥感卫星主要有 SCanning Imaging Absorption spectrometer for Atmospheric Cartography (SCIAMACHY)/ENVironmental SATellite (ENVISAT)、Sentinel-5P/TROPOMI、The Greenhouse gases Observing Satellite (GOSAT) 等。为实现对甲烷柱浓度的精确观测, 光谱分辨率要较高 ( $0.3 \text{ nm}$  以内), 波段要更为集中在甲烷吸收窗口, 因此主要对大尺度、长时序的甲烷排放情况进行研究。

2003 年, 搭载于欧洲空间局环境卫星 ENVISAT 升空的 SCIAMACHY 是首个能够灵敏检测到边界层  $\text{CH}_4$  变化的星载传感器, 但 2005 年开始性能严重退化 (信噪比小于 100), 其探测精度难以满足需求<sup>[20]</sup>。文献<sup>[21-22]</sup>使用 SCIAMACHY 数据分别研究了油气生产区的甲烷排放。2009 年, 日本 GOSAT 卫星成功发射, 其热红外和近红外傅里叶变换光谱仪 (TANSO-FTS) 观测的数据被广泛用来检测全球温室气体<sup>[23-26]</sup>。其继任者 GOSAT-2 于 2018 年发射, 两者均可每隔 3 天覆盖全球一次, 但每次观测的是约为  $10 \text{ km}$  直径的单个圆形像元, 且像元之间间隔约  $270 \text{ km}$ , 数据较为稀疏。目前, GOSAT 卫星提供了可追溯到 2009 年的连续且经过良好校准 (空间可变偏差为  $2.9 \times 10^{-9} \text{ m}^3/\text{m}^3$ ) 的甲烷数据集, 已用于煤炭甲烷的贡献归因中<sup>[17,27]</sup>。2017 年, 搭载于 S5P 发射的 TROPOMI 可提供具有  $7 \text{ km} \times 7 \text{ km}$  分辨率 (自 2019 年 8 月 6 日提升至  $5.5 \text{ km} \times 7 \text{ km}$ ) 的完整每日全球覆盖范围的大气甲烷观测数据。TROPOMI 已经广泛用于区域尺度的煤炭行业甲烷排放研究<sup>[28-30]</sup>, 且有研究将其用于澳大利亚昆士兰州煤矿甲烷超强排放羽流的检测和量化<sup>[28]</sup>。

针对煤炭行业点源甲烷排放监测目标的遥感卫星代表是 GHGSat-D, 其每次观测约  $12 \text{ km}^2$  的区域, 空间分辨率达  $25 \text{ m}$ , 在全球众多煤矿排放检测方面取得了实质性进展<sup>[18,31]</sup>。此外, 科学家们发现原本用于对地观测的高空间分辨率 ( $3.7\sim 60 \text{ m}$ ) 成像仪在宽吸收波段 ( $2.3 \mu\text{m}$ ) 同样具有检测甲烷羽流的能力, 包括: 具有约  $10 \text{ nm}$  光谱分辨率的星载高光谱传感器, 如我国 GF-5A、GF-5B 与资源一号 02D 星 (ZY-1 02D) 载有的 Advanced Hyperspectral Imager (AHSI)<sup>[32-34]</sup>、意大利的 PRISMA<sup>[35-36]</sup>、德国的 EnMAP<sup>[37]</sup>、美国的 Earth Surface Mineral Dust Source Investigation (EMIT)<sup>[38]</sup>; 甚至是可以利用多光谱传感器单个  $2.3 \mu\text{m}$  通道或结合其相邻通道进行反演的传感器, 如 Sentinel-2A/2B<sup>[39-40]</sup>、WorldView-3<sup>[41-42]</sup> 等, 但受光谱分辨率低的限制, 此类传感器通常只适用于反演超级排放源的甲烷浓度增强信号。表 1 是目前可用于煤炭行业甲烷排放研究的在轨遥感卫星, 可分为用于区域甲烷排放研究的遥感卫星 (GOSAT、GOSAT-2、Sentinel-5P)、用于点源甲烷排放研究的高光谱遥感卫星 (GF-5、ZY-1E、GHGSat-D、PRISMA、EnMAP、EMIT)、用于点源甲烷排放研究的多光谱遥感卫星 (Sentinel-2A、Sentinel-2B、WorldView-3)。

## 3 煤炭行业甲烷柱浓度遥感反演进展

### 3.1 区域尺度的 $\text{XCH}_4$ 遥感反演

SCIAMACHY、TROPOMI、GOSAT 等区域型卫星传感器的甲烷柱浓度反演是通过将观测光谱拟合到模拟光谱来估算甲烷垂直柱浓度 ( $\Omega_{\text{CH}_4}$ ) 实现的, 为了消除地表压强变化造成的影响, 通常将  $\Omega_{\text{CH}_4}$  除以干空气柱浓度  $\Omega_{\text{air}}$  的步骤转为干空气柱平均混合比  $X_{\text{CH}_4}$  计算, 根据仪器具体配置的波段差异, 可使用全物理反演和  $\text{CO}_2$  代理法这两大类算法。

全物理反演方法建立在遥感物理的基础上, 将反演问题变成非线性代数方程求解问题, 地表和大气的散射特性将作为反演的一部分参与拟合, 此类过程又可使用直接最优估计 (OE) 和基于差分吸收光谱 (DOAS) 的反演这两种方案。

1) OE 反演是一个普适的定量遥感反演方案<sup>[43]</sup>, 其借助辐射传输模型模拟得到的辐亮度和遥感实际观测的辐亮度之间的差异和先验廓线值来定义代价函数, 利用迭代方式来逐步逼近真解, 得到的结果即为最优估计值 (或称后验值)。大气遥感的正演过程 (或称前向模拟) 通过正演算子  $F$  (如辐射传输模型) 将一组给定的测量值  $y$  (如短波红外范围内的光谱辐亮度) 与大气参数  $x$  (如甲烷的垂直分布) 联系起来:

$$y = F(x, b) + \epsilon I, \quad (1)$$

式中:  $b$  是除甲烷外的其他先验参数, 包括卫星观测几何、地表特性、云和气溶胶的特性等;  $\epsilon$  为误差项;  $I$  为单

表 1 可用于煤炭行业甲烷排放研究的在轨遥感卫星

Table 1 On orbit remote sensing satellites for studying methane emissions in the coal industry

Satellite/Sensor	Data phase	Transit time	Substellar point resolution	Inverted band / $\mu\text{m}$	Spectral resolution /nm	Revisit period /d
GOSAT/TANSO-FTS	2009—	13:00	10.5 km [diameter]	1.65	0.06	3
GOSAT-2/TANSO-FTS-2	2018—	13:00	9.7 km [diameter]	1.65, 2.3	0.06	3
Sentinel-5P/TROPOMI	2017—	13:30	5.5 km $\times$ 7 km [7 km $\times$ 7 km]	2.3	0.25	1
GF-5/AHSI	2018—	13:30	30 m $\times$ 30 m	1.65	10	2
ZY-1E/AHSI	2019—	10:30	30 m $\times$ 30 m	1.65	20	5
GHGSat-D/WAF-P	2016—	09:30	25 m $\times$ 25 m	1.65	0.3	1—7
PRISMA/HYC	2019—	10:30	30 m $\times$ 30 m	2.3	<12	4
EnMAP/HSI	2022—	11:00	30 m $\times$ 30 m	2.3	10	4
EMIT/ Imaging Spectrometer	2022—	11:00	60 m $\times$ 60 m	2.3	9	3
Sentinel-2A/MSI	2015—	10:30	20 m $\times$ 20 m	2.3	200	2-5
Sentinel-2B/MSI	2017—	10:30	20 m $\times$ 20 m	2.3	200	2-5
WorldView-3/WV110-Camera	2014—	13:30	3.7 m $\times$ 3.7 m	2.3	50	<1

位矩阵。但  $F$  的逆过程无法从  $\mathbf{y}$  得到唯一的  $x$  (此问题或称为“病态反演”), 此时可将式 (1) 转换为在给定  $\mathbf{y}$  的情况下求解  $x$  的最大似然估计值  $\hat{x}$  的计算。根据贝叶斯理论可知, 后验概率密度函数  $P(x|\mathbf{y})$  服从于  $P(x)P(\mathbf{y}|x)$ , 若假设误差服从高斯分布, 则可定义代价函数 (或称损失函数) 为

$$J(x) = [\mathbf{y} - F(x, b)]^T S_\epsilon^{-1} [\mathbf{y} - F(x, b)] + [x - x_a]^T S_a^{-1} [x - x_a], \quad (2)$$

式中:  $x_a$  为甲烷的先验廓线;  $S_a$  为先验廓线的误差协方差矩阵;  $S_\epsilon$  为卫星探测器噪声协方差矩阵。在  $J(x)$  导数为 0 时, 将解得的  $x$  代入式 (2), 可使得  $J(x)$  取极小值, 此时的  $x$  即为待求的  $\hat{x}$ 。在计算机中实现此过程需要借助以下迭代算法:

$$x_{(i+1)} = x_{(i)} + (K^T S_\epsilon^{-1} K)^{-1} \{ K^T S_\epsilon^{-1} [\mathbf{y} - F(x_{(i)}, b) - S_a^{-1} (x_{(i)} - x_a)] \}, \quad (3)$$

式中:  $K$  为前向模型在  $x_{(i)}$  处的 Jacobian 矩阵 (或称权重函数), 即辐亮度对甲烷浓度变化的敏感性。

2) DOAS 技术<sup>[44]</sup> 广泛应用于二氧化氮、二氧化硫、甲醛等紫外可见光波段痕量气体柱浓度的反演中。它将大气消光分为瑞利散射、云和气溶胶消光等的宽带结构 (随波长缓慢变化, 可通过低阶多项式近似的方法去除) 和痕量气体的窄带吸收结构 (随波长变化快), 且能够实现对多组分的同时求解。其理论基础为 Beer-Lambert 定律<sup>[45]</sup>, 即散射辐射强度  $L$  随光路长度指数下降, 表达式为

$$L(\lambda) = L_0(\lambda) \cdot e^{-\int_0^s \sigma(\lambda, P, T) c(s) ds}, \quad (4)$$

式中:  $L_0$  表示光束的初始强度 (被动遥感采用太阳参考谱);  $\sigma(\lambda, P, T)$  为吸收参考光谱在波长  $\lambda$ 、压强  $P$ 、

温度  $T$  处的吸收截面;  $c(s)$  为痕量气体在光程  $s$  处的浓度。对于二氧化氮这类弱吸收气体, 其光程不受浓度影响, 且与压强的相关性较小, 此时可直接对需要积分的各项进行累加, 得到一个线性方程组, 则剩下的窄带贡献可利用最小二乘法进行直接拟合以获得沿大气光路积分的痕量气体斜柱浓度。然而红外吸收光谱是分子振动和转动跃迁引起的, 其吸收谱线相当窄, 并且强烈依赖于温度和压力<sup>[46]</sup>, 此时  $\sigma(\lambda, P, T)$  沿光路  $ds$  不是常数, 因此不能简化式 (4) 中的积分项, 即常规的 DOAS 方法并不适用于温室气体的反演。

为修正温度、压强对吸收截面的影响, 德国不莱梅大学开发了加权函数修正差分吸收光谱算法 (WFM-DOAS)<sup>[47]</sup>, 波长  $\lambda$  处观测的辐射强度的对数被近似为辐射传输模型模拟值对数的一阶泰勒展开式加上一个低阶多项式, 这意味着原来的吸收截面项被柱浓度加权函数取代, 之后通过最小二乘拟合可直接得到甲烷垂直总柱浓度。该算法最早用于 SCIAMACHY 数据的反演中, 目前针对 TROPOMI 也发布了一套科研产品<sup>[48]</sup>, 目前已发布 1.8 版本, 随机误差降低至  $12.4 \times 10^{-9} \text{ m}^3/\text{m}^3$ , 系统性误差为  $5.2 \times 10^{-9} \text{ m}^3/\text{m}^3$ , 由于使用的是  $2.3 \mu\text{m}$  波段, 该算法还可同时快速反演出一氧化碳柱浓度。德国海德堡大学提出了一种改进的基于最优估计理论的迭代最大后验 DOAS (IMAP-DOAS) 算法<sup>[46]</sup>, 该方法通过将原先 OE 反演使用的辐射传输模型前向模型换为基于 Beer-Lambert 定律的前向模型来计算 Jacobian 矩阵, 同样直接迭代甲烷的柱浓度, 直到式 (4) 模拟的辐亮度与遥感观测值吻合。DOAS 类算法的核心是利用低阶多项式拟合来去除气溶胶等的散射作用, 在实际应用中这种拟合并不完全符合大气辐

射传输过程,会造成反演结果的误差。但对于一般不产生气溶胶的甲烷排放点源,其影响较小,不过仍需要晴空的观测条件<sup>[49]</sup>。

CO<sub>2</sub>代理法则假定大气散射以相同的方式影响CH<sub>4</sub>和CO<sub>2</sub>吸收的光路,从而在光谱拟合时忽略掉大气散射的影响<sup>[50]</sup>。由于CO<sub>2</sub>在1.61 μm波段存在吸收窗口,而波长相近时吸收强度相似,故对于配有1.65 μm观测波段的传感器,可在不考虑大气散射的情况下同时反演出两种气体的柱浓度Ω<sub>CH<sub>4</sub></sub>和Ω<sub>CO<sub>2</sub></sub>,然后利用两者的比率抵消大气散射的影响。此时,X<sub>CH<sub>4</sub></sub>的表达式为

$$X_{CH_4} = \frac{\Omega_{CH_4}}{\Omega_{CO_2}} \times X_{CO_2}, \quad (5)$$

式中:X<sub>CO<sub>2</sub></sub>通常由全球大气化学传输模型或同化观测后的再分析资料提供<sup>[51-52]</sup>,不依赖待反演传感器的单次观测结果,而是利用大气中CO<sub>2</sub>的变化远小于CH<sub>4</sub>的特点得到的。

与全物理方法的反演结果的对比表明,CO<sub>2</sub>代理法精度和准确度与之相当,但计算效率更高,且很大程度上避免了与地表反射率和气溶胶有关的偏差,尤为适用于煤矿等CO<sub>2</sub>排放量较低的甲烷源研究<sup>[53-54]</sup>。TROPOMI业务化运行使用的是荷兰空间研究所

(SRON)开发的RemoToC<sup>[55-56]</sup>全物理算法。日本国家环境研究所(NIES)开发的GOSAT业务化产品采用的是全物理算法<sup>[57]</sup>。SRON和英国莱斯特大学均提供了CO<sub>2</sub>代理法和全物理法两套GOSAT甲烷科研产品数据。

如图1(a)和图1(b)所示,TROPOMI(SRON全物理算法产品)和GOSAT(莱斯特大学CO<sub>2</sub>代理法产品)CH<sub>4</sub>数据在山西煤矿区的均值大概为1920×10<sup>-9</sup>~1960×10<sup>-9</sup> m<sup>3</sup>/m<sup>3</sup>,这远低于同期的地面原位观测结果(3304×10<sup>-9</sup> m<sup>3</sup>/m<sup>3</sup>左右)<sup>[58]</sup>。虽然已有验证结果表明TROPOMI和GOSAT的精度令人满意,例如文献<sup>[25]</sup>基于2018年5月到2019年4月的21个全球地基傅里叶变换光谱仪网络TCCON站点的数据对比发现,全球范围的TROPOMI和GOSAT的CH<sub>4</sub>数据偏差分别仅为-2.7×10<sup>-9</sup> m<sup>3</sup>/m<sup>3</sup>和-1.0×10<sup>-9</sup> m<sup>3</sup>/m<sup>3</sup>,但是,TCCON<sup>[59]</sup>在煤矿区没有站点,无法验证TROPOMI和GOSAT的甲烷数据在煤矿排放场景下的表现。同时,如图1(c)所示,煤矿地区的X<sub>CH<sub>4</sub></sub>标准差显著高于周边地区,表明煤矿排放的逐日变化性很强。进一步,从图2可知:TROPOMI在山西煤矿区的X<sub>CH<sub>4</sub></sub>产品数据覆盖率仅有30%~40%;而GOSAT数据仅以零星点存在,基本无法用于月、日尺度的排放研究。

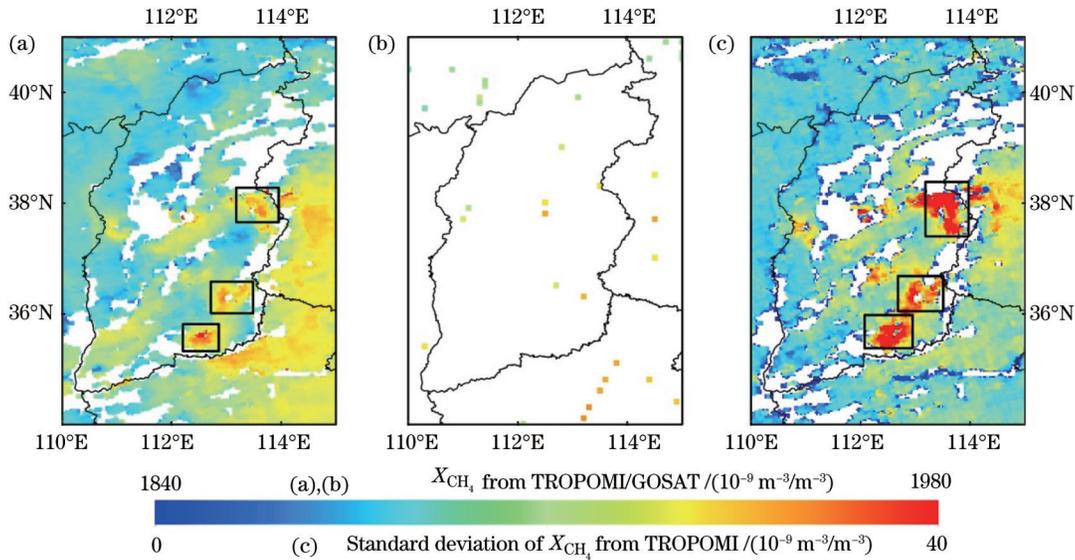


图1 2021年10月到12月煤炭产量大省山西及周边地区的卫星数据,矩形框显示的是阳泉、长治、晋城3个主要的煤矿地区。(a) TROPOMI甲烷柱浓度均值;(b)GOSAT甲烷柱浓度均值;(c)TROPOMI甲烷柱浓度标准差

Fig.1 Satellite data of Shanxi, a major coal-producing province, and surrounding areas from October to December 2021, the rectangular boxes show the three main coal mining areas of Yangquan, Changzhi, and Jincheng. (a) Mean column concentration of methane from TROPOMI; (b) mean column concentration of methane from GOSAT; (c) standard deviation of column concentration of methane from TROPOMI

### 3.2 点源尺度的ΔX<sub>CH<sub>4</sub></sub>遥感反演

针对煤矿点源排放目标的遥感卫星可以分为高光谱和多光谱两类:前者包括光谱分辨率为0.3 nm的GHGSat-D和10 nm的AHSI、PRISMA、EnMAP;后者有Sentinel-2 A/2B、Landsat-8/9、WorldView-3等。

GHGSat-D搭载了一台光谱范围为1630~1675 nm的微型法布里-珀罗干涉仪,采用全物理算法反演甲烷干空气柱体积混合比增量ΔX<sub>CH<sub>4</sub></sub>。首先,使用全物理OE算法反演整个场景范围内的平均浓度,为下一步线性化正演模型的状态向量提供初始浓度值,

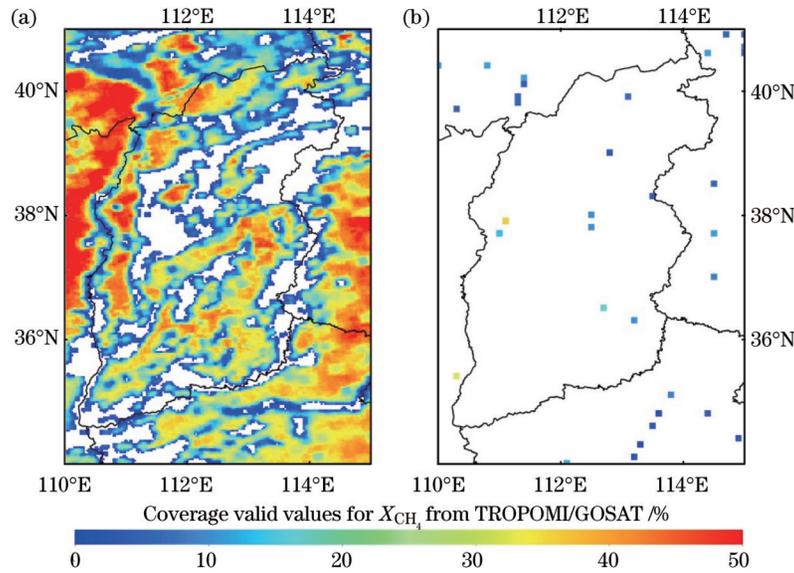


图 2 2021 年 10 月到 12 月煤炭产量大省山西及周边地区的  $X_{CH_4}$  产品数据总体覆盖率(有数据的天数占所有天数的比例)。(a) TROPOMI 覆盖率;(b)GOSAT 覆盖率

Fig. 2 Overall coverage of  $X_{CH_4}$  product data (the ratio of days with data to all days) of Shanxi, a major coal-producing province, and surrounding areas from October to December 2021. (a) TROPOMI coverage; (b) GOSAT coverage

由此反演逐像元的甲烷浓度,最终减去背景浓度(即 OE 算法中的场景平均浓度)得到整个空间每个像元的甲烷浓度增大值。

AHSI、PRISMA、EnMAP 采用的是匹配滤波法<sup>[60-62]</sup>。由于每个输入光谱都可以表示为无甲烷增强环境中传感器接收到的辐亮度加上甲烷柱浓度变化引起的辐射扰动的结果,因此可先建立目标光谱,即单位甲烷吸收在各波长引起的辐射信号增强值,然后将观测光谱拟合到与目标光谱卷积的背景光谱上,即可解得甲烷点源柱浓度相对于周围背景的背景光谱上,即可解得甲烷点源柱浓度相对于周围背景的逐像元增强值。匹配滤波方法可直接得到相较于背景区域的甲烷增强值,并且速度远超全物理算法,尤其适用于高分辨率的遥感观测数据,但是对于地表反射率较大的区域,其反演结果可能存在伪影(或称假阳性),此时需要结合风场和地表等先验知识进行人工剔除<sup>[63]</sup>。在高浓度气溶胶场景中,匹配滤波法比全物理算法对甲烷浓度的低估更严重<sup>[64]</sup>。文献[65]借助匹配滤波法生成的甲烷羽流样本,利用深度学习中的 Mask R-CNN 来对目标进行检测,训练好的模型能够以更快速度得到甲烷羽流结果,同时减少了检测结果中假阳性的比例。文献[66]应用了迭代对数正态匹配滤波器方法<sup>[67]</sup>来应对传统匹配滤波器对强甲烷羽流排放量化的低估。

Sentinel-2 A/2B、Landsat-8/9、WorldView-3 等多光谱类遥感卫星使用单一的  $2.3 \mu\text{m}$  波段及其相邻波段,光谱响应范围较宽(约  $100\sim 200 \text{ nm}$ ),无法利用高光谱吸收线逐一拟合的方式进行  $X_{CH_4}$  反演。研究人员主要利用相邻波段具有相似的地表反射率和气溶胶散射、甲烷吸收特性不同的特点,组合几种甲烷排放场景或者相邻波段<sup>[39-42]</sup>,在 Beer-Lambert 定律基础上来推

断羽流中相对于背景增强的  $\Delta X_{CH_4}$ 。

$$L = L_{ref} \cdot e^{-F_{AMF} \cdot \sigma_{CH_4} \cdot \Delta X_{CH_4}}, \quad (6)$$

式中: $L$  和  $L_{ref}$  分别代表甲烷敏感波段/场景和无甲烷参考波段/场景下的辐射率; $\sigma_{CH_4}$  指甲烷吸收截面。 $F_{AMF}$  指大气质量因子,在不考虑大气散射时即为几何大气质量因子,只与太阳高度角  $\theta_{SZA}$  和卫星天顶角  $\theta_{VZA}$  有关,表达式为

$$F_{AMF} = \frac{1}{\cos \theta_{SZA}} + \frac{1}{\cos \theta_{VZA}}. \quad (7)$$

因此,可利用两个辐射率和  $\Delta X_{CH_4}$  的关联构建查找表,

$$\Delta X_{CH_4} = \frac{-\ln(L/L_{ref})}{F_{AMF} \cdot \sigma_{CH_4}}, \quad (8)$$

实际上, $L/L_{ref}$  为甲烷透过率, $-\ln(L/L_{ref})$  为甲烷吸收率,或称为光学厚度,两者的选取可采用如下方式:一个波段甲烷强吸收、另一个相邻波段甲烷表现为弱吸收;同一区域一个时刻有甲烷羽流、另一个时刻没有甲烷排放;既考虑波段又考虑是否存在排放。

## 4 煤炭行业甲烷排放速率遥感反演进展

根据卫星观测数据识别甲烷排放的尺度差异性,对煤炭行业甲烷排放速率的估算主要有两种不同的方法:区域型遥感卫星通常借助大气化学模型来反演优化区域尺度下甲烷排放的二维分布;点源遥感卫星则通过甲烷排放烟羽的质量守恒分析来估算单个点源排放速率,其中点源一般是在小于  $30 \text{ m} \times 30 \text{ m}$  区域内排放超过  $10 \text{ kg/h}$  的单一设施<sup>[68]</sup>。

### 4.1 区域甲烷排放速率遥感反演

区域甲烷排放速率遥感反演一般采用卫星观测与

正向模型后验估计方法,即通过大气化学模型(正向模型)模拟大气成分的传输、光学、沉降、混合等过程,以排放清单作为先验信息,利用观测对排放的敏感度,通过贝叶斯定律求解优化的排放估计(后验估计)<sup>[69]</sup>,其本质是求解连续性方程以满足质量守恒:

$$\frac{\partial C}{\partial t} = \nabla(Cv) + E - L, \quad (9)$$

式中: $C$ 为甲烷浓度; $v$ 为三维风场; $\nabla(Cv)$ 为传输项; $E$ 为排放速率; $L$ 为损失项,主要包括对流层中与OH的氧化(约占总汇的77%)、平流层损失(约占总汇的7%)、通气良好的干燥土壤中的生物氧化(约占总汇的4%)<sup>[70]</sup>。对于全球长期的大气化学模型模拟,须考虑该损失项,因为其于对流层OH反应消耗的量可达528 Tg/a<sup>[71]</sup>,不加考虑可能无法满足质量守恒定律;但是对于嵌套区域的甲烷排放反演,往往忽略该项,其时间尺度比甲烷存续时间短得多,因为模拟的时候受到边界条件(指初始的浓度和边界场的浓度值)的限制,所以不会显著增加排放量<sup>[50]</sup>。

采用贝叶斯定理获得后验排放概率密度函数的最大值,其流程与遥感最优估计反演甲烷柱浓度类似。原先式(1)中的状态向量 $x$ 由甲烷柱浓度变为先验排放清单中的甲烷排放速率,此时 $x$ 的维度 $n$ 由各个卫星波段变为各个空间网格,观测向量 $y$ 由传感器接收的辐亮度转为卫星反演得到的甲烷浓度,正向算子 $F$ 由辐射传输模型变为大气化学模型。由于不考虑化学损失的非线性影响, $x$ 与 $y$ 之间近似为线性关系,原先式(2)中 $F$ 可用Jacobian矩阵 $K = \partial y / \partial x$ 来代替, $K$ 从前向模型对每个网格单元中的排放进行扰动得到计算。当 $\nabla_x J(x)$ 为0时, $J(x)$ 取极小值,此时后验排放值 $\hat{x}$ 、后验误差协方差矩阵 $\hat{S}$ 、平均核(averaging kernel)矩阵 $A$ 分别为

$$\hat{x} = x_a + S_a K^T (K S_a K^T + S_e)^{-1} (y - K x_a), \quad (10)$$

$$\hat{S} = (K^T S_e^{-1} K + S_a^{-1}) (K^T S_e^{-1} K + S_a^{-1})^{-1}, \quad (11)$$

$$A = I_n - \hat{S} S_a^{-1}, \quad (12)$$

式中: $I_n$ 为 $n$ 维单位矩阵; $x_a$ 为甲烷排放清单提供的先验甲烷排放速率; $S_a$ 为先验排放的误差协方差矩阵,可通过对比多个清单的差异<sup>[72]</sup>或利用单一清单自身提供的不确定度<sup>[73]</sup>来构造; $S_e$ 为观测误差协方差矩阵,包括仪器和传输模型误差,可以采用残差法对观测值与有先验排放估计的大气模型模拟浓度进行比较,去除平均偏差后的残差作为观测误差<sup>[74]</sup>。 $A$ 即 $\partial \hat{x} / \partial x$ ,其对角项(从0到1)称为平均核灵敏度,可衡量观测值约束该状态向量元素的解的能力(1表示完全约束,0表示完全没有)。 $A$ 的迹(trace)称为信号的自由度(DOFS),表示从观测中可以完全约束的信息的总数。

一系列反演方法是在此基础上得到了优化:加入正则化系数 $\gamma$ 来校正误差项构造中不完善引起的过拟合<sup>[75-76]</sup>;将先验排放信息作为排放的相对空间分布而

不是网格化的排放速率来使用<sup>[77]</sup>;将先验排放误差呈高斯分布的假设替换为对数正态分布来估计点源密集区的甲烷排放<sup>[78]</sup>;但也有研究认为对数正态分布仍然低估了超级排放点源的量,故改用双峰概率密度函数,并将L1范数替换为L2范数来构造代价函数<sup>[79]</sup>。

以上方法主要采用解析解的方式来求算,虽然需要在大型计算集群上扰动先验排放来运行大气化学模型构造 $K$ ,但一旦构建完成,就可以在不显著增加计算成本的情况下进行反演,同时还能够得到反演参数的不确定性,并检查不同卫星仪器或地面站点数据的互补性和一致性<sup>[76]</sup>。但该方法仍受限于模拟的区域范围和空间分辨率大小,对状态向量的维度有限制,因此部分研究使用数值解的方式,如大气化学模型伴随模式<sup>[80]</sup>或变分方法<sup>[81]</sup>,避免显式构建 $K$ ,以满足任何维度状态向量的反演,不过在推导 $\hat{S}$ 时需要额外的计算开销。

此外,为了获取贝叶斯逆问题(BIP)的后验分布,还有研究使用卡尔曼滤波器(KF)<sup>[82-83]</sup>或马尔可夫链蒙特卡罗(MCMC)<sup>[84]</sup>求解。KF的优势在于能够对排放的时间趋势进行优化,从而得到逐月甚至逐周的排放;而MCMC无须指定概率密度函数类型,通过大批次的随机采样来模拟数据的实际分布,适用于含有排放量较大点源的场景,因为它们往往具有厚尾(fat tailed)分布特征。

卫星观测与正向模型后验估计方法需要借助大气化学模型,其运算开销大,对计算资源要求高,且空间分辨率较大,同时先验清单对结果影响较大。从图3(a)和图3(b)可知,采用卫星观测与正向模型后验估计方法得到的排放结果与图3(c)的逐个煤矿排放清单相比,空间分辨率过大且缺失的排放较多。一些研究者尝试拓展了针对短存续时间痕量气体排放量反演的轻量级方法<sup>[85-86]</sup>。尽管提到的甲烷平均存续时间远小于CO<sub>2</sub>,但相比NO<sub>2</sub>这样小时尺度的短存续气体,背景浓度较高,受传输和地形的影响较大,因此首先需要去除背景浓度得到增强值(或称异常值),再运用相应的轻量级方法进行反演。文献[87-88]运用羽流旋转法得到排放源上风向的平均背景浓度(此过程还考虑了季节循环和日变化因素),在此基础上再各自利用高斯积分法或锥形烟羽扩散模型进行拟合,得到排放量。文献[89]将没有甲烷先验排放场景下模拟的甲烷浓度视为平流层浓度,用卫星反演的总柱浓度减去平流层浓度得到边界层内排放产生的浓度,并将研究区域浓度的十分位数作为背景浓度来剥离。在稳态情况下,式(9)中 $\partial C / \partial t$ 和 $L$ 为0,此时排放项等于散度项,因而无须借助任何关于排放强度与空间位置的先验数据即可直接求解,但这类方法均对风场信息要求较高,尤其是复杂地形上的风速问题欠考虑。本团队提出的卫星观测约束的简化质量平衡方法保留了卫星遥感产

品数据的原始分辨率,已成功应用于氮氧化物排放估算中<sup>[90-91]</sup>。

#### 4.2 点源甲烷排放速率遥感反演

卫星遥感单次观测的高分辨率甲烷瞬时羽流的形态由叠加在平均风场的湍流扩散决定,可以在采取高斯滤波对  $\Delta X_{CH_4}$  进行平滑去噪后,以滤波结果的中位数作为阈值进行像元分割,来提取出羽流掩模区域,在此基础上量化点源的排放速率。高斯烟羽扩散模型是点源湍流扩散的经典模型,即假设烟羽沿风向稳定均匀三维展开,在稳定的大气中烟羽主要在水平方向扩散,而对流条件有利于垂直扩散<sup>[92]</sup>。实际中,甲烷羽流通常太小,无法满足这样的假设,只适用于具有代表性的湍流涡流类型<sup>[93]</sup>。高斯理论模型(或称散度积分法)直接计算沿点源周围轮廓的外向通量总和<sup>[94-95]</sup>,广泛用于机载走航观测,尤其具备风廓线雷达记录准确风

场信息的场景。但是该方法一方面没有考虑湍流扩散对外向通量的贡献,另一方面又将区域内任何排放源的贡献混在一起<sup>[63]</sup>。

截面通量(CSF)法<sup>[96]</sup>和质量增强积分(IME)法<sup>[97]</sup>是两种广泛使用的从瞬时烟羽观测获得点源排放速率的方法,且两者估算结果具有较高的一致性<sup>[18]</sup>。CSF方法对羽流掩模区域边界之间的  $\Delta X_{CH_4}$  进行积分,并对下风向不同距离处横截面计算排放速率,之后取均值来减小误差;IME方法则对羽流掩模区域每个像元的  $\Delta X_{CH_4}$  乘上对应的面积,然后除以羽流扩散距离  $L_d$  (通常取羽流掩模区域面积的平方根)再乘上有效风速  $U_{eff}$ 。两者都需要使用与烟羽输送有关的风速:CSF方法利用烟羽垂直高度上的平均风速,可以从 10 m 风速<sup>[98]</sup>进行参数化,也可以从风速垂直廓线数据库进行插值;IME方法利用有效风速  $U_{eff}$ ,考虑了烟羽耗散中

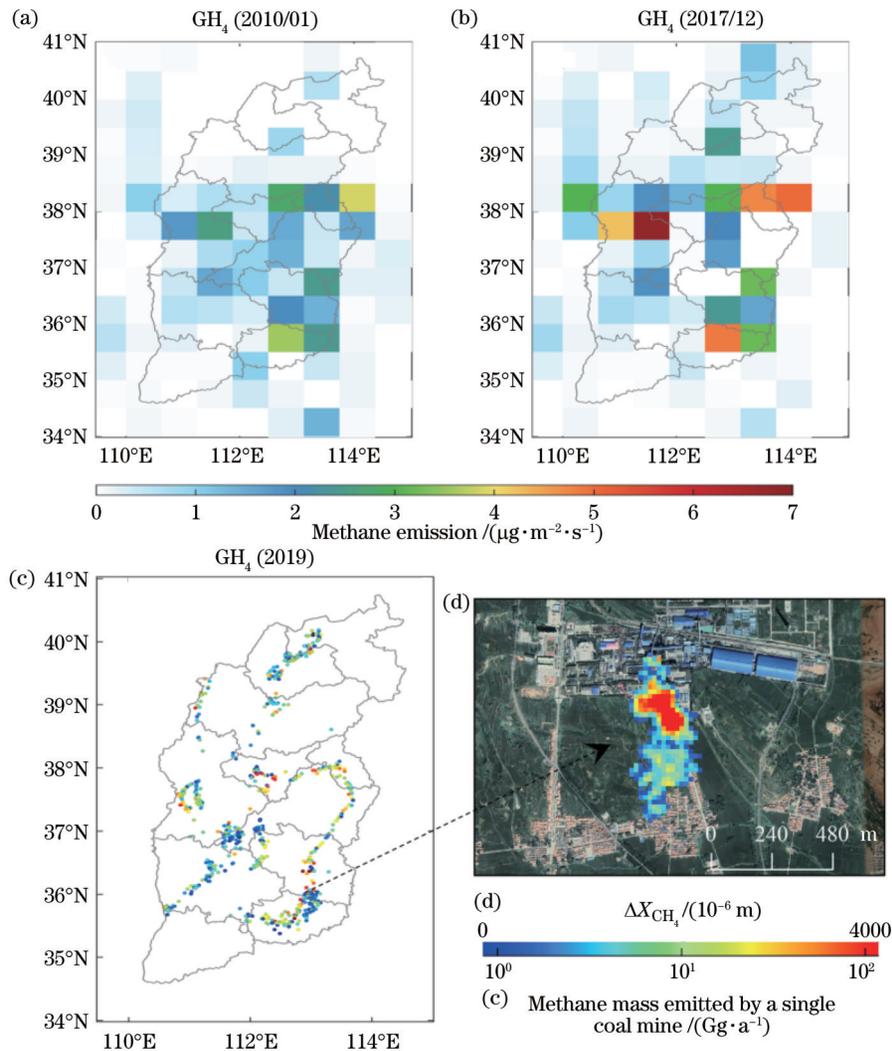


图 3 多尺度下的煤矿甲烷排放。(a)(b)GOSAT 和 GEOS-Chem 模式估算的山西省煤炭行业的甲烷排放<sup>[17]</sup>;(c)本团队通过地面观测的约束自下而上逐个煤矿反演甲烷排放;(d)采用 GF-5B/AHSI 数据反演的煤矿甲烷羽流增强浓度  $\Delta X_{CH_4}$ 。

Fig. 3 Methane emissions from coal mines at multiple scales. (a) (b) Methane emissions from the coal industry in Shanxi province estimated by GOSAT and GEOS-Chem model<sup>[17]</sup>; (c) methane emissions from individual coal mines by our team using a bottom-up inversion constrained by ground observations; (d) methane plume enhancement concentration  $\Delta X_{CH_4}$  from coal mines inverted by GF-5B/AHSI data

湍流扩散的影响,可对大涡模拟(LES)合成的烟羽进行参数化,得到其与再分析资料中 10 m 风速的函数关系。CSF 和 IME 方法不确定度的 30% 受限于风场数据信息的影响,且对风速有一定限制(10 m 风速在 2~5 m/s 最为合适)<sup>[98]</sup>,虽然弱风条件有利于检测到烟羽,但在量化点源排放速率方面会引起很大的误差,强风下烟羽稀释后不易被探测到。图 3(d)为本团队使用 GF-5B/AHSI 数据和 IME 方法检测反演得到的山西长治地区某个年产 800 万吨煤大型煤矿的甲烷羽流。

## 5 结论与展望

通过梳理国内外煤炭行业甲烷卫星遥感检测与排放量化研究进展,可以总结出两点结论。

1) 当前可用于煤炭行业甲烷排放研究的区域型遥感卫星主要是 TROPOMI 和 GOSAT/GOSAT-2,并以全物理法和 CO<sub>2</sub>代理法为主反演得到 X<sub>CH<sub>4</sub></sub>。目前的 X<sub>CH<sub>4</sub></sub> 产品数据在我国煤矿区存在系统性的低估,逐日变化较大,表明煤炭行业的甲烷排放研究需要高频次的卫星观测,数据覆盖率低限制了后续的逐日、逐月排放研究。卫星观测与正向模型后验估计方法是区域甲烷排放速率遥感反演的主要方法,但其受到大气化学传输模式的分辨率限制和先验清单的缺失或不准确的影响较大。2) 针对单一煤矿尺度的点源排放目标的遥感卫星有高光谱成像仪和多光谱仪两类。前者中的 GHGSat-D 光谱分辨率更高,而 AHSI、PRISMA、EnMAP 等光谱分辨率较低,分别采用全物理法和匹配滤波法反演煤矿排放羽流中相对背景的甲烷增强信号 ΔX<sub>CH<sub>4</sub></sub>,进一步采用 CSF 方法和 IME 方法估算排放速率。后者有 Sentinel-2A/B、Landsat-8/9、WorldView-3 等,但它们仅适用于超级排放源,用于煤矿甲烷排放检测难度较大。

相较于农业中的排放源,煤炭行业的甲烷排放有两个显著的特点。1) 排放强度与煤矿生产活动密切相关,例如综采工作时瓦斯排出多,巷道掘进时瓦斯排出少;安全生产检查时比正常生产时排放少。因此,煤矿甲烷排放检测对卫星遥感观测的时间频次要求更高,仅靠单一过境卫星的观测数据,容易低估或高估排放量。2) 我国煤矿绝大多数为井工开采方式,巷道里的甲烷可通过风井、抽采站、煤层气开采井等多个分散的地面设施排出,对卫星观测的空间分辨率要求更高。因此,基于现有的遥感卫星技术,建议从煤矿聚集区和单一煤矿两个尺度加快构建“自上而下”的中国煤炭行业排放清单,重点开展以下 3 个方面的针对性研究。

1) 采用 TROPOMI 和简化质量平衡法反演全国 14 个大型煤炭基地的甲烷排放

针对全国 14 个大型煤炭基地(神东、陕北、黄陇、晋北、晋中、晋东、蒙东(东北)、两淮、鲁西、河南、冀中、

云贵、宁东、新疆)<sup>[99]</sup>,使用当前 X<sub>CH<sub>4</sub></sub> 数据覆盖率最佳的 TROPOMI 开展区域尺度的甲烷排放检测与估算研究。为突破大气化学传输模式的空间分辨率限制,引入本团队提出的简化质量平衡方法<sup>[90-91]</sup>。该方法不依赖庞大复杂的大气化学模式而是通过卫星观测与先验清单或地面原位观测的参数进行拟合来求算排放,更加突出观测数据的贡献,保留卫星产品数据的原始分辨率,实现 0.05°×0.05°分辨率的甲烷排放快速反演。

2) 基于 10 nm 分辨率的高光谱遥感卫星检测量化全国数千家煤矿的甲烷排放

虽然 GHGSat-D 在单一煤矿的甲烷排放检测和量化中表现突出,但鉴于其商业卫星属性获取成本高,而 AHSI、PRISMA、EnMAP、EMIT 等 10 nm 分辨率的高光谱遥感卫星的光谱数据对研究人员免费开放,用它们开展全国数千家煤矿的甲烷排放研究有经济可行性。由于单一煤矿的地表甲烷增强幅度较大,其精度要求无须像进行区域观测的亚纳米传感器严格,但在地表异质性较高情况下常测到甲烷伪影特征,故还需要人工目视检查判断是否此处有煤矿、羽流扩散方向是否与风向一致、地表反射率是否过高来筛选伪影。但是,对于位于山区或盆地的煤矿,很多时候风场变化迅速,非单一风向,在遥感卫星观测数据中难以形成规则的羽流,会出现非线性风切变导致的浓度增加而不是点源排放的现象。例如,文献<sup>[93]</sup>的研究表明,观测到的甲烷烟羽形态实际上包含着风场信息:因为细长形态的烟羽通常出现在高风速情况下,而短粗烟羽与低风速相关。在这种情景下,可以考虑本团队提出的简化质量平衡方法<sup>[90-91]</sup>。

此外,深度学习在机载遥感甲烷羽流探测、排放速率估算方面也崭露头角<sup>[100,65]</sup>,因推断速度快、自动化程度高、不依赖额外风场数据的优势,其有利于部署在系统中实现对全国数千家煤矿的甲烷羽流探测。但目前该方法仅在机载传感器上实现,它能否运行星载传感器进行大范围、不同光照角度下的观测还需进一步检验。

3) 挖掘不同尺度的遥感卫星观测数据之间的内在联系开展协同分析

鉴于煤矿甲烷排放的高度时间变化性和空间异质性,增加卫星观测频次有助于逼近真实排放特征,发射新型静止卫星或用相似的传感器组成卫星星座固然是一个可采取的策略,但考虑到经济成本因素和技术约束,短期内较难实现。由于不同尺度的观测和了解甲烷排放是互补的,大量单独的小型排放源如低瓦斯煤矿可以累积成大的总量,整合在一个大的像元中<sup>[101]</sup>,因此,需要区域和点源遥感观测的联动协同,基于煤矿聚集区和单一煤矿的排放之间的时空关联性,充分挖掘同一研究区域的 TROPOMI 与 AHSI、PRISMA、

EnMAP 等观测数据之间的内在联系。例如,文献[102]发现全球甲烷排放事件遵循幂律分布,可以通过检测大的排放源推断出小排放源的数量,从而估算出总排放量;文献[40]证明该幂律模型在二叠纪盆地这样的区域尺度上同样适用。

## 参 考 文 献

- [1] IEA. International energy agency[EB/OL]. [2023-03-05]. [https://iea.blob.core.windows.net/assets/efa961c4-ac83-4a9c-88ee-62c0bd9ff2e9/DrivingDownCoalMineMethaneEmissions\\_Chinese.pdf](https://iea.blob.core.windows.net/assets/efa961c4-ac83-4a9c-88ee-62c0bd9ff2e9/DrivingDownCoalMineMethaneEmissions_Chinese.pdf).
- [2] IPCC. Climate Change 2014: Synthesis Report. Contribution of Working Groups I, II and III to the fifth assessment report of the intergovernmental panel on climate change[R]. [2023-03-05]. [https://www.ipcc.ch/site/assets/uploads/2018/02/AR5\\_SYR\\_FINAL\\_Front\\_matters.pdf](https://www.ipcc.ch/site/assets/uploads/2018/02/AR5_SYR_FINAL_Front_matters.pdf).
- [3] Prather M J, Holmes C D, Hsu J. Reactive greenhouse gas scenarios: systematic exploration of uncertainties and the role of atmospheric chemistry[J]. *Geophysical Research Letters*, 2012, 39(9): L09803.
- [4] Moore B III, Braswell B H. The lifetime of excess atmospheric carbon dioxide[J]. *Global Biogeochemical Cycles*, 1994, 8(1): 23-38.
- [5] Archer D, Eby M, Brovkin V, et al. Atmospheric lifetime of fossil fuel carbon dioxide[J]. *Annual Review of Earth and Planetary Sciences*, 2009, 37: 117-134.
- [6] Control methane to slow global warming—fast[J]. *Nature*, 2021, 596(7873): 461.
- [7] Abernethy S, O' Connor F M, Jones C D, et al. Methane removal and the proportional reductions in surface temperature and ozone[J]. *Philosophical Transactions of the Royal Society A: Mathematical, Physical and Engineering Sciences*, 2021, 379(2210): 20210104.
- [8] Francoeur C B, McDonald B C, Gilman J B, et al. Quantifying methane and ozone precursor emissions from oil and gas production regions across the contiguous US[J]. *Environmental Science & Technology*, 2021, 55(13): 9129-9139.
- [9] 中美关于在 21 世纪 20 年代强化气候行动的格拉斯哥联合宣言[EB/OL]. [2023-03-05]. [https://www.gov.cn/xinwen/2021-11/11/content\\_5650318.htm](https://www.gov.cn/xinwen/2021-11/11/content_5650318.htm).  
Glasgow Joint Declaration between China and the United States on Strengthening Climate Action in the 2020s[EB/OL]. [2023-03-05]. [https://www.gov.cn/xinwen/2021-11/11/content\\_5650318.htm](https://www.gov.cn/xinwen/2021-11/11/content_5650318.htm).
- [10] 马翠梅,戴尔卓,刘乙辰,等.中国煤炭开采和矿后活动甲烷逃逸排放研究[J].*资源科学*, 2020, 42(2): 311-322.  
Ma C M, Dai E F, Liu Y C, et al. Methane fugitive emissions from coal mining and post-mining activities in China[J]. *Resources Science*, 2020, 42(2): 311-322.
- [11] 中华人民共和国气候变化第二次两年更新报告[EB/OL]. [2022-10-03]. <http://big5.mee.gov.cn/gate/big5/www.mee.gov.cn/ywgz/ydqhbh/wsqtzk/201907/P020190701765971866571.pdf>.  
Second Biennial Update Report on Climate Change in the People's Republic of China[EB/OL]. [2022-10-03]. <http://big5.mee.gov.cn/gate/big5/www.mee.gov.cn/ywgz/ydqhbh/wsqtzk/201907/P020190701765971866571.pdf>.
- [12] Saunio M, Bousquet P, Poulter B, et al. The global methane budget 2000—2012[J]. *Earth System Science Data*, 2016, 8(2): 697-751.
- [13] Miller S M, Michalak A M, Detmers R G, et al. China's coal mine methane regulations have not curbed growing emissions[J]. *Nature Communications*, 2019, 10: 303.
- [14] Gao J L, Guan C H, Zhang B. China's CH<sub>4</sub> emissions from coal mining: a review of current bottom-up inventories[J]. *Science of the Total Environment*, 2020, 725: 138295.
- [15] 邓剑波.短波红外卫星遥感甲烷大气柱平均干空气混合比反演算法研究[D].北京:中国科学院大学,2015.  
Deng J B. Research on inversion algorithm for average dry air mixing ratio of methane atmospheric column using short wave infrared satellite remote sensing[D]. Beijing: University of Chinese Academy of Sciences, 2015.
- [16] 何卓,李正强,樊程,等.大气甲烷卫星传感器和遥感算法研究综述[J].*光学学报*, 2023, 43(18): 1800002.  
He Z, Li Z Q, Fan C, et al. Satellite sensors and retrieval algorithms of atmospheric methane[J]. *Acta Optica Sinica*, 43(18): 1800002.
- [17] Zhang Y Z, Fang S X, Chen J M, et al. Observed changes in China's methane emissions linked to policy drivers[J]. *Proceedings of the National Academy of Sciences of the United States of America*, 2022, 119(41): e2202742119.
- [18] Varon D J, Jacob D J, Jervis D, et al. Quantifying time-averaged methane emissions from individual coal mine vents with GHGSat-D satellite observations[J]. *Environmental Science & Technology*, 2020, 54(16): 10246-10253.
- [19] 姚璐,杨东旭,蔡兆男,等.面向我国碳中和、碳达峰的大气甲烷观测卫星现状与发展趋势分析[J].*大气科学*, 2022, 46(6): 1469-1483.  
Yao L, Yang D X, Cai Z N, et al. Present situation and development trend analysis of atmospheric methane observation satellites for China's carbon neutrality and peak carbon dioxide emissions[J]. *Chinese Journal of Atmospheric Sciences*, 2022, 46(6): 1469-1483.
- [20] Frankenberg C, Aben I, Bergamaschi P, et al. Global column-averaged methane mixing ratios from 2003 to 2009 as derived from SCIAMACHY: trends and variability[J]. *Journal of Geophysical Research: Atmospheres*, 2011, 116(D4): JD014849.
- [21] Schneising O, Burrows J P, Dickerson R R, et al. Remote sensing of fugitive methane emissions from oil and gas production in North American tight geologic formations[J]. *Earth's Future*, 2014, 2(10): 548-558.
- [22] Kort E A, Frankenberg C, Costigan K R, et al. Four corners: the largest US methane anomaly viewed from space[J]. *Geophysical Research Letters*, 2014, 41(19): 6898-6903.
- [23] Butz A, Guerlet S, Hasekamp O P, et al. Using ocean-glint scattered sunlight as a diagnostic tool for satellite remote sensing of greenhouse gases[J]. *Atmospheric Measurement Techniques*, 2013, 6(9): 2509-2520.
- [24] Zhang Y Z, Jacob D J, Lu X, et al. Attribution of the accelerating increase in atmospheric methane during 2010—2018 by inverse analysis of GOSAT observations[J]. *Atmospheric Chemistry and Physics*, 2021, 21(5): 3643-3666.
- [25] Qu Z, Jacob D J, Shen L, et al. Global distribution of methane emissions: a comparative inverse analysis of observations from the TROPOMI and GOSAT satellite instruments[J]. *Atmospheric Chemistry and Physics*, 2021, 21(18): 14159-14175.
- [26] Wang F J, Maksyutov S, Janardanan R, et al. Interannual variability on methane emissions in monsoon Asia derived from GOSAT and surface observations[J]. *Environmental Research Letters*, 2021, 16(2): 024040.
- [27] Sheng J X, Tunnicliffe R, Ganesan A L, et al. Sustained methane emissions from China after 2012 despite declining coal production and rice-cultivated area[J]. *Environmental Research Letters*, 2021, 16(10): 104018.
- [28] Sadavarte P, Pandey S, Maasackers J D, et al. Methane emissions from superemitting coal mines in Australia quantified using TROPOMI satellite observations[J]. *Environmental Science & Technology*, 2021, 55(24): 16573-16580.
- [29] Chen Z C, Jacob D J, Nesser H, et al. Methane emissions from

- China: a high-resolution inversion of TROPOMI satellite observations[J]. *Atmospheric Chemistry and Physics*, 2022, 22(16): 10809-10826.
- [30] Tu Q S, Schneider M, Hase F, et al. Quantifying CH<sub>4</sub> emissions in hard coal mines from TROPOMI and IASI observations using the wind-assigned anomaly method[J]. *Atmospheric Chemistry and Physics*, 2022, 22(15): 9747-9765.
- [31] Liang R, Zhang Y, Chen W, et al. East Asian methane emissions inferred from high-resolution inversions of GOSAT and TROPOMI observations: a comparative and evaluative analysis[J]. *Atmospheric Chemistry and Physics*, 2023, 23(14): 8039-8057.
- [32] 徐涵秋, 孙凤琴, 徐光志. 高分五号卫星高光谱 AHSI 和多光谱 VIMI 传感器辐亮度数据的交互对比[J]. *武汉大学学报(信息科学版)*, 2021, 46(7): 1032-1043.
- Xu H Q, Sun F Q, Xu G Z. Cross comparison of radiance data between hyperspectral AHSI and multispectral VIMI sensors of Gaofen-5 satellite[J]. *Geomatics and Information Science of Wuhan University*, 2021, 46(7): 1032-1043.
- [33] Irakulis-Loitxate I, Guanter L, Liu Y N, et al. Satellite-based survey of extreme methane emissions in the Permian Basin[J]. *Science Advances*, 2021, 7(27): eabf4507.
- [34] 李飞, 孙世玮, 张永光, 等. 高分五号 02 星高光谱成像仪中美典型甲烷超级排放源遥感反演与分析[J/OL]. *遥感学报*, 2023: 1-15[2023-02-03]. <https://www.ygxb.ac.cn/zh/article/doi/10.11834/jrs.20232453/>.
- Li F, Sun S W, Zhang Y G, et al. Mapping methane super-emitters in China and United States with GF5-02 hyperspectral imaging spectrometer[J/OL]. *National Remote Sensing Bulletin*, 2023: 1-15[2023-02-03]. <https://www.ygxb.ac.cn/zh/article/doi/10.11834/jrs.20232453/>.
- [35] Nesme N, Marion R, Lezeaux O, et al. Joint use of in-scene background radiance estimation and optimal estimation methods for quantifying methane emissions using PRISMA hyperspectral satellite data: application to the korpezhe industrial site[J]. *Remote Sensing*, 2021, 13(24): 4992.
- [36] Guanter L, Irakulis-Loitxate I, Gorrño J, et al. Mapping methane point emissions with the PRISMA spaceborne imaging spectrometer[J]. *Remote Sensing of Environment*, 2021, 265: 112671.
- [37] Guanter L, Kaufmann H, Segl K, et al. The EnMAP spaceborne imaging spectroscopy mission for earth observation [J]. *Remote Sensing*, 2015, 7(7): 8830-8857.
- [38] Cusworth D H, Jacob D J, Varon D J, et al. Potential of next-generation imaging spectrometers to detect and quantify methane point sources from space[J]. *Atmospheric Measurement Techniques*, 2019, 12(10): 5655-5668.
- [39] Varon D J, Jervis D, McKeever J, et al. High-frequency monitoring of anomalous methane point sources with multispectral Sentinel-2 satellite observations[J]. *Atmospheric Measurement Techniques*, 2021, 14(4): 2771-2785.
- [40] Ehret T, de Truchis A, Mazzolini M, et al. Global tracking and quantification of oil and gas methane emissions from recurrent Sentinel-2 imagery[J]. *Environmental Science & Technology*, 2022, 56(14): 10517-10529.
- [41] Irakulis-Loitxate I, Gorrño J, Zavala-Araiza D, et al. Satellites detect a methane ultra-emission event from an offshore platform in the gulf of Mexico[J]. *Environmental Science & Technology Letters*, 2022, 9(6): 520-525.
- [42] Sánchez-García E, Gorrño J, Irakulis-Loitxate I, et al. Mapping methane plumes at very high spatial resolution with the WorldView-3 satellite[J]. *Atmospheric Measurement Techniques*, 2022, 15(6): 1657-1674.
- [43] Rodgers C D. *Inverse methods for atmospheric sounding: theory and practice*[M]. Singapore: World Scientific, 2000.
- [44] Platt U, Perner D, Pätz H W. Simultaneous measurement of atmospheric CH<sub>2</sub>O, O<sub>3</sub>, and NO<sub>2</sub> by differential optical absorption[J]. *Journal of Geophysical Research: Oceans*, 1979, 84(C10): 6329-6335.
- [45] Swinehart D F. The Beer-Lambert law[J]. *Journal of Chemical Education*, 1962, 39(7): 333.
- [46] Frankenberg C, Platt U, Wagner T. Iterative maximum a posteriori (IMAP)-DOAS for retrieval of strongly absorbing trace gases: model studies for CH<sub>4</sub> and CO<sub>2</sub> retrieval from near infrared spectra of SCIAMACHY onboard ENVISAT[J]. *Atmospheric Chemistry and Physics*, 2005, 5(1): 9-22.
- [47] Buchwitz M, Rozanov V V, Burrows J P. A near-infrared optimized DOAS method for the fast global retrieval of atmospheric CH<sub>4</sub>, CO, CO<sub>2</sub>, H<sub>2</sub>O, and N<sub>2</sub>O total column amounts from SCIAMACHY Envisat-1 nadir radiances[J]. *Journal of Geophysical Research: Atmospheres*, 2000, 105(D12): 15231-15245.
- [48] Schneising O, Buchwitz M, Reuter M, et al. A scientific algorithm to simultaneously retrieve carbon monoxide and methane from TROPOMI onboard Sentinel-5 Precursor[J]. *Atmospheric Measurement Techniques*, 2019, 12(12): 6771-6802.
- [49] Thorpe A K, Frankenberg C, Roberts D A. Retrieval techniques for airborne imaging of methane concentrations using high spatial and moderate spectral resolution: application to AVIRIS[J]. *Atmospheric Measurement Techniques*, 2014, 7(2): 491-506.
- [50] Jacob D J, Turner A J, Maasackers J D, et al. Satellite observations of atmospheric methane and their value for quantifying methane emissions[J]. *Atmospheric Chemistry and Physics*, 2016, 16(22): 14371-14396.
- [51] Parker R J, Webb A, Boesch H, et al. A decade of GOSAT Proxy satellite CH<sub>4</sub> observations[J]. *Earth System Science Data*, 2020, 12(4): 3383-3412.
- [52] Parker R J, Boesch H, Byckling K, et al. Assessing 5 years of GOSAT Proxy XCH<sub>4</sub> data and associated uncertainties[J]. *Atmospheric Measurement Techniques*, 2015, 8(11): 4785-4801.
- [53] Buchwitz M, Reuter M, Schneising O, et al. The Greenhouse Gas Climate Change Initiative (GHG-CCI): comparison and quality assessment of near-surface-sensitive satellite-derived CO<sub>2</sub> and CH<sub>4</sub> global data sets[J]. *Remote Sensing of Environment*, 2015, 162: 344-362.
- [54] Schepers D, Guerlet S, Butz A, et al. Methane retrievals from Greenhouse Gases Observing Satellite (GOSAT) shortwave infrared measurements: performance comparison of proxy and physics retrieval algorithms[J]. *Journal of Geophysical Research: Atmospheres*, 2012, 117(D10): D017549.
- [55] Hu H L, Landgraf J, Detmers R, et al. Toward global mapping of methane with TROPOMI: first results and intersatellite comparison to GOSAT[J]. *Geophysical Research Letters*, 2018, 45(8): 3682-3689.
- [56] Hu H L, Hasekamp O, Butz A, et al. The operational methane retrieval algorithm for TROPOMI[J]. *Atmospheric Measurement Techniques*, 2016, 9(11): 5423-5440.
- [57] Yoshida Y, Kikuchi N, Morino I, et al. Improvement of the retrieval algorithm for GOSAT SWIR XCO<sub>2</sub> and XCH<sub>4</sub> and their validation using TCCON data[J]. *Atmospheric Measurement Techniques*, 2013, 6(6): 1533-1547.
- [58] 刘艳秋, 秦凯, 科恩·杰森, 等. 基于涡动及走航观测的晋东南煤矿区甲烷分布特征[J]. *煤炭学报*, 2022, 47(12): 4395-4402.
- Liu Y Q, Qin K, Cohen J, et al. Distribution characteristics of methane in southeastern Shanxi coal mining area based on eddy current and navigation observation[J]. *Journal of China Coal Society*, 2022, 47(12): 4395-4402.
- [59] Toon G, Blavier J F, Washenfelder R, et al. Total column carbon observing network (TCCON) [C]//*Hyperspectral Imaging and Sensing of the Environment 2009*, April 26-30, 2009, Vancouver, Canada. Washington, D. C.: Optica

- Publishing Group, 2009: JMA3.
- [60] Thompson D R, Leifer I, Bovensmann H, et al. Real-time remote detection and measurement for airborne imaging spectroscopy: a case study with methane[J]. *Atmospheric Measurement Techniques*, 2015, 8(10): 4383-4397.
- [61] Foote M D, Dennison P E, Thorpe A K, et al. Fast and accurate retrieval of methane concentration from imaging spectrometer data using sparsity prior[J]. *IEEE Transactions on Geoscience and Remote Sensing*, 2020, 58(9): 6480-6492.
- [62] Foote M D, Dennison P E, Sullivan P R, et al. Impact of scene-specific enhancement spectra on matched filter greenhouse gas retrievals from imaging spectroscopy[J]. *Remote Sensing of Environment*, 2021, 264: 112574.
- [63] Jacob D J, Varon D J, Cusworth D H, et al. Quantifying methane emissions from the global scale down to point sources using satellite observations of atmospheric methane[J]. *Atmospheric Chemistry and Physics*, 2022, 22(14): 9617-9646.
- [64] Huang Y X, Natraj V, Zeng Z C, et al. Quantifying the impact of aerosol scattering on the retrieval of methane from airborne remote sensing measurements[J]. *Atmospheric Measurement Techniques*, 2020, 13(12): 6755-6769.
- [65] Kumar S, Torres C, Ulutan O, et al. Deep remote sensing methods for methane detection in overhead hyperspectral imagery [C]//2020 IEEE Winter Conference on Applications of Computer Vision (WACV), March 1-5, 2020, Snowmass, CO, USA. New York: IEEE Press, 2020: 1765-1774.
- [66] Pei Z P, Han G, Mao H Q, et al. Improving quantification of methane point source emissions from imaging spectroscopy[J]. *Remote Sensing of Environment*, 2023, 295: 113652.
- [67] Schaum A. A uniformly most powerful detector of gas plumes against a cluttered background[J]. *Remote Sensing of Environment*, 2021, 260: 112443.
- [68] Duren R M, Thorpe A K, Foster K T, et al. California's methane super-emitters[J]. *Nature*, 2019, 575(7781): 180-184.
- [69] Brasseur G P, Jacob D J. *Modeling of atmospheric chemistry* [M]. Cambridge: Cambridge University Press, 2017.
- [70] Whalen S C, Reeburgh W S. Consumption of atmospheric methane by tundra soils[J]. *Nature*, 1990, 346(6280): 160-162.
- [71] 张定媛, 廖宏. 大气甲烷的源和汇及其浓度的观测模拟研究进展[J]. *气象科技进展*, 2015, 5(1): 40-47.
- Zhang D Y, Liao H. Advances in the research on sources and sinks of CH<sub>4</sub> and observations and simulations of CH<sub>4</sub> concentrations[J]. *Advances in Meteorological Science and Technology*, 2015, 5(1): 40-47.
- [72] Bloom A A, Bowman K W, Lee M, et al. A global wetland methane emissions and uncertainty dataset for atmospheric chemical transport models (WetCHARTs version 1.0) [J]. *Geoscientific Model Development*, 2017, 10(6): 2141-2156.
- [73] Scarpelli T R, Jacob D J, Maasakkers J D, et al. A global gridded (0.1° × 0.1°) inventory of methane emissions from oil, gas, and coal exploitation based on national reports to the United Nations Framework Convention on Climate Change[J]. *Earth System Science Data*, 2020, 12(1): 563-575.
- [74] Wecht K J, Jacob D J, Frankenberg C, et al. Mapping of North American methane emissions with high spatial resolution by inversion of SCIAMACHY satellite data[J]. *Journal of Geophysical Research: Atmospheres*, 2014, 119(12): 7741-7756.
- [75] Lu X A, Jacob D J, Zhang Y Z, et al. Global methane budget and trend, 2010—2017: complementarity of inverse analyses using *in situ* (GLOBALVIEWplus CH<sub>4</sub> ObsPack) and satellite (GOSAT) observations[J]. *Atmospheric Chemistry and Physics*, 2021, 21(6): 4637-4657.
- [76] Shen L, Zavala-Araiza D, Gautam R, et al. Unravelling a large methane emission discrepancy in Mexico using satellite observations[J]. *Remote Sensing of Environment*, 2021, 260: 112461.
- [77] Miller S M, Saibaba A K, Trudeau M E, et al. Geostatistical inverse modeling with very large datasets: an example from the Orbiting Carbon Observatory 2 (OCO-2) satellite[J]. *Geoscientific Model Development*, 2020, 13(3): 1771-1785.
- [78] Yuan B, Kaser L, Karl T, et al. Airborne flux measurements of methane and volatile organic compounds over the Haynesville and Marcellus shale gas production regions[J]. *Journal of Geophysical Research: Atmospheres*, 2015, 120(12): 6271-6289.
- [79] Cusworth D H, Jacob D J, Sheng J X, et al. Detecting high-emitting methane sources in oil/gas fields using satellite observations[J]. *Atmospheric Chemistry and Physics*, 2018, 18(23): 16885-16896.
- [80] Cho T, Chung J, Miller S M, et al. Computationally efficient methods for large-scale atmospheric inverse modeling[J]. *Geoscientific Model Development*, 2022, 15(14): 5547-5565.
- [81] Bousserez N, Henze D K, Perkins A, et al. Improved analysis-error covariance matrix for high-dimensional variational inversions: application to source estimation using a 3D atmospheric transport model[J]. *Quarterly Journal of the Royal Meteorological Society*, 2015, 141(690): 1906-1921.
- [82] Varon D J, Jacob D J, Hmiel B, et al. Continuous weekly monitoring of methane emissions from the Permian Basin by inversion of TROPOMI satellite observations[J]. *Atmospheric Chemistry and Physics*, 2023, 23(13): 7503-7520.
- [83] Feng L A, Palmer P I, Bösch H, et al. Consistent regional fluxes of CH<sub>4</sub> and CO<sub>2</sub> inferred from GOSAT proxy XCH<sub>4</sub>: XCO<sub>2</sub> retrievals, 2010—2014[J]. *Atmospheric Chemistry and Physics*, 2017, 17(7): 4781-4797.
- [84] Western L M, Ramsden A E, Ganesan A L, et al. Estimates of North African methane emissions from 2010 to 2017 using GOSAT observations[J]. *Environmental Science & Technology Letters*, 2021, 8(8): 626-632.
- [85] Beirle S, Borger C, Dörner S, et al. Pinpointing nitrogen oxide emissions from space[J]. *Science Advances*, 2019, 5(11): eaax9800.
- [86] Beirle S, Boersma K F, Platt U, et al. Megacity emissions and lifetimes of nitrogen oxides probed from space[J]. *Science*, 2011, 333(6050): 1737-1739.
- [87] Tu Q S, Hase F, Schneider M, et al. Quantification of CH<sub>4</sub> emissions from waste disposal sites near the city of Madrid using ground- and space-based observations of COCCON, TROPOMI and IASI[J]. *Atmospheric Chemistry and Physics*, 2022, 22(1): 295-317.
- [88] Schneising O, Buchwitz M, Reuter M, et al. Remote sensing of methane leakage from natural gas and petroleum systems revisited[J]. *Atmospheric Chemistry and Physics*, 2020, 20(15): 9169-9182.
- [89] Liu M Y, van der A R, van Weele M, et al. A new divergence method to quantify methane emissions using observations of Sentinel-5P TROPOMI[J]. *Geophysical Research Letters*, 2021, 48(18): e2021GL094151.
- [90] Li X, Cohen J B, Qin K, et al. Remotely sensed and surface measurement derived mass-conserving inversion of daily high-resolution NO<sub>x</sub> emissions and inferred combustion technologies in energy rich Northern China[EB/OL]. [2023-07-16]. <https://egusphere.copernicus.org/preprints/2023/egusphere-2023-2/>.
- [91] Qin K, Lu L X, Liu J, et al. Model-free daily inversion of NO<sub>x</sub> emissions using TROPOMI (MCMFE-NO<sub>x</sub>) and its uncertainty: declining regulated emissions and growth of new sources[J]. *Remote Sensing of Environment*, 2023, 295: 113720.
- [92] Matheou G, Bowman K W. A recycling method for the large-eddy simulation of plumes in the atmospheric boundary layer[J]. *Environmental Fluid Mechanics*, 2016, 16(1): 69-85.
- [93] Jongaramrungruang S, Frankenberg C, Matheou G, et al. Towards accurate methane point-source quantification from high-

- resolution 2-D plume imagery[J]. *Atmospheric Measurement Techniques*, 2019, 12(12): 6667-6681.
- [94] Chulakadabba A, Sargent M, Lauvaux T, et al. Methane point source quantification using MethaneAIR: a new airborne imaging spectrometer[EB/OL]. (2023-04-29) [2023-05-04]. <https://egusphere.copernicus.org/preprints/2023/egusphere-2023-822/egusphere-2023-822-supplement.pdf>.
- [95] Hajny K D, Salmon O E, Rudek J, et al. Observations of methane emissions from natural gas-fired power plants[J]. *Environmental Science & Technology*, 2019, 53(15): 8976-8984.
- [96] Krings T, Gerilowski K, Buchwitz M, et al. MAMAP – a new spectrometer system for column-averaged methane and carbon dioxide observations from aircraft: retrieval algorithm and first inversions for point source emission rates[J]. *Atmospheric Measurement Techniques*, 2011, 4(9): 1735-1758.
- [97] Frankenberg C, Thorpe A K, Thompson D R, et al. Airborne methane remote measurements reveal heavy-tail flux distribution in Four Corners region[J]. *Proceedings of the National Academy of Sciences of the United States of America*, 2016, 113(35): 9734-9739.
- [98] Varon D J, Jacob D J, McKeever J, et al. Quantifying methane point sources from fine-scale satellite observations of atmospheric methane plumes[J]. *Atmospheric Measurement Techniques*, 2018, 11(10): 5673-5686.
- [99] 丁国峰, 吕振福, 曹进成, 等. 我国大型煤炭基地开发利用现状分析[J]. *能源与环保*, 2020, 42(11): 107-110, 120. Ding G F, Lü Z F, Cao J C, et al. Analysis on status quo of development and utilization of large-scale coal bases in China[J]. *China Energy and Environmental Protection*, 2020, 42(11): 107-110, 120.
- [100] Jongaramrungruang S, Thorpe A K, Matheou G, et al. MethaNet-an AI-driven approach to quantifying methane point-source emission from high-resolution 2-D plume imagery[J]. *Remote Sensing of Environment*, 2022, 269: 112809.
- [101] Omara M, Zavala-Araiza D, Lyon D R, et al. Methane emissions from US low production oil and natural gas well sites [J]. *Nature Communications*, 2022, 13: 2085.
- [102] Lauvaux T, Giron C, Mazzolini M, et al. Global assessment of oil and gas methane ultra-emitters[J]. *Science*, 2022, 375(6580): 557-561.

## Progress and Prospect of Satellite Remote Sensing Research Applied to Methane Emissions from the Coal Industry

Qin Kai\*, He Qin, Kang Hanshu, Hu Wei, Lu Fan, Cohen Jason

*Jiangsu Key Laboratory of Coal-Based Greenhouse Gas Control and Utilization, School of Environment and Spatial Informatics, China University of Mining and Technology, Xuzhou 221116, Jiangsu, China*

### Abstract

**Significance** Methane is a significant and powerful greenhouse gas, with a global warming potential over 80 times than that of carbon dioxide over a 20-year time scale. At the same time, methane decomposes much faster than carbon dioxide, with an average lifespan (namely, the duration an emitted molecule of methane stays in the atmosphere) of about 12 years, compared with hundreds of years for carbon dioxide. This means that compared with a reduction of carbon dioxide, a reduction of methane emissions can offer more control over the greenhouse effect, including controls on global average temperature rise in the short term. In addition, methane is also a precursor of both tropospheric ozone and carbon monoxide. Therefore, a reduction in its emissions will help reduce air pollution and improve air quality.

During coal mining activities, the methane contained in the coal seam is released in a variety of ways, including escape from the coal seam in open pit mines, discharge through ventilation and drainage in underground coal mines, and release from pockets trapped in the coal matrix during mining. Escape continues during post-operation activities and coal processing. Methane in abandoned mine shafts also continues to escape from coal remaining after operations. According to data from the International Energy Agency, in 2022, global coal mine methane emissions were about 40.5 million tons, accounting for more than 10% of total anthropogenic methane emissions. China is the largest coal producer in the world. According to the 2014 National Greenhouse Gas Inventory of the Second Biennial Update Report on Climate Change in China, methane emissions from the country's energy industry accounted for about 46% of the total emissions, mainly attributed to coal emissions from mining. Studies have shown that the increase in global anthropogenic methane emissions from 2000 to 2012 and the increase in China's methane emissions from 2010 to 2015 are both significantly impacted by China's coal mining industry. Accelerating the establishment of a dynamically updateable high-spatial-resolution methane emission inventory for the coal industry is an important starting point for promoting methane emission reductions in the coal industry.

Using the short-wave infrared absorption spectrum of methane at 1.65  $\mu\text{m}$  and 2.3  $\mu\text{m}$ , satellite remote sensing technology has been successfully used in the detection and quantification of methane emissions in the coal industry. Satellite remote sensing detection of methane emissions in the coal industry requires close cooperation between sensors,

algorithms, and detection targets. We analyze the research progress from the aspects of remote sensing satellites that can be used for the study of methane emissions in the coal industry, the corresponding methane column concentration, and emission rate inversion technology, and propose a satellite remote sensing method for building a high-spatial-resolution methane emission inventory of China's coal industry research focus.

**Progress** The spatial scale of the methane emission capacity of the coal industry detected by remote sensing satellites has been previously divided into regional and point source types (Table 1). Regional remote sensing satellites mainly include SCIAMACHY/ENVISAT, Sentinel-5P/TROPOMI, GOSAT, etc. In order to realize the accurate observation of methane concentration, its spectral resolution is higher (within 0.3 nm), and the band is more concentrated in the methane absorption window, so it is mainly aimed at the study of spatially large-scale and temporally long-term methane emission sources. GHGSat-D is the representative remote sensing satellite for point source methane emission targeting the coal industry. It observes an area of about 12 km<sup>2</sup> at a time, with a spatial resolution of 25 m. Substantial progress has been made in the detection of emissions from many coal mines around the world. In addition, the scientists found that the high spatial resolution (3.7–60 m) imager originally used for Earth observation also can detect methane plumes in its broad absorption (2.3 μm) band.

The methane column concentration inversion of regional satellite sensors such as SCIAMACHY, TROPOMI, and GOSAT estimates the atmospheric methane column concentration  $\Omega_{\text{CH}_4}$  by fitting the observed spectrum to its simulated spectrum. In order to eliminate the influence of surface pressure changes, the column mass is first normalized by the dry air column concentration  $\Omega_{\text{air}}$ , yielding the dry air column average mixing ratio  $X_{\text{CH}_4}$ . According to the band difference of the specific configuration of the instrument, two types of algorithms, namely the full physical inversion and the CO<sub>2</sub> proxy method, can be used. Remote sensing satellites for coal mine point source emissions can be divided into hyperspectral type and multispectral type. The former includes GHGSat-D with a spectral resolution of 0.3 nm and AHSI, PRISMA, and EnMAP with a spectral resolution of 10 nm; the latter includes Sentinel-2 A/2B, Landsat-8/9, WorldView-3, etc.

According to the spatial scale of methane emissions identified by satellite observation data, there are two main methods for estimating the methane emission rate of the coal industry: regional remote sensing satellites usually use atmospheric chemical models to invert and optimize the two-dimensional distribution of methane emissions on a regional scale, while point source remote sensing satellites estimate the emission rate of a single point source through mass conservation of methane emissions within a plume-model assumption, where a point source is generally a single facility that emits more than 10 kg/h in an area less than 3 × 30 m<sup>2</sup>.

**Conclusions and Prospects** This work recommends speeding up the construction of a "top-down" emission inventory of China's coal industry from two different scales: coal mine agglomerations and single coal mines. This work further points out three weaknesses that need to be focused on and improved in the future: 1) simplified mass balance methods using TROPOMI observations to constrain and retrieve the methane emissions over 14 large coal bases across the country; 2) detection and quantification of the methane emissions of thousands of coal mines across the country based on hyperspectral remote sensing satellites with 10 nm resolution; 3) more closely examining the internal links between remote sensing satellite observations at different scales and other observations collaboratively and analytically.

**Key words** methane; coal mine; emission; TROPOMI satellite; GF-5 satellite